Med Bio Eng Comput (2007) 45:421–435
DOI 10.1007/s11517-007-0170-5

REVIEW ARTICLE

Laser Doppler perfusion monitoring and imaging: novel approaches

Anne Humeau · Wiendelt Steenbergen · Henrik Nilsson · Tomas Strömberg

Received: 6 November 2006 / Accepted: 5 December 2006 / Published online: 6 March 2007

Abstract Laser Doppler flowmetry (LDF) is a non invasive method enabling the monitoring of microvascular blood flow, a very important marker of tissue health. This article gives an overview on the concept of LDF for microvascular perfusion monitoring and imaging. It first describes the theoretical background of the technique. Then, the benefits of LDF signal processing are shown through clinical examples: use of time–frequency representations and wavelets. Afterwards, the paper introduces novel approaches of velocity components. For that purpose, a work providing the determination of the velocities relative contribution in physiologically relevant units (mm/s) is presented. Imaging perfusion is also reviewed through methods based on laser speckle. The most prominent disadvantage of the latter devices being the time needed to produce a perfusion image, solutions are proposed in the last part of the paper.

Keywords Laser Doppler flowmetry · Perfusion · Microcirculation · Monitoring · Imaging

A. Humeau (✉)
Groupe ISAIP-ESAIP, 18 rue du 8 mai 1945, BP 80022,
49180 Saint Barthélémy d'Anjou cedex, France
e-mail: ahumeau@isaip.uco.fr

A. Humeau
Laboratoire d'Ingénierie des Systèmes Automatisées (LISA),
Université d'Angers, 62 avenue Notre Dame du Lac,
49000 Angers, France

H. Nilsson
MedLeap ApS, Cort Adelersgade 4,
1053 Copenhagen K, Denmark

W. Steenbergen
Faculty of Science and Technology, Biophysical Engineering
Group, University of Twente, PO Box 217,
7500 AE Enschede, The Netherlands

T. Strömberg
Department of Biomedical Engineering,
Linköpings Universitet, 581 85 Linköping, Sweden

1 Introduction

Laser Doppler flowmetry (LDF) is a non invasive method enabling the monitoring of microvascular blood flow. Even though LDF measures are non-absolute, the enormous interest in microvascular perfusion has led to many clinical works and a number of international papers related to the technique. Indeed, it can be used in many disciplines and on many organs, such as skin, brain, kidney, liver, and intestines [2, 40, 49, 50, 58].

The perfusion in the skin relates the blood flow in the microcirculation. Microcirculation is composed of capillaries, arterioles (small arteries), venules (small veins), and arteriovenous anastomosis (shunting vessels). The perfusion through capillaries refers to the nutritive flow, whereas flow through the other mentioned vessels (arterioles, venules and shunting vessels) refers to the temperature regulation flow, and also feed and drain the capillary network. However, skin perfusion can be impaired by diseases. These impairments can lead to ulcer formations as well as necrosis. That is why tools aiming at monitoring skin blood perfusion in real time, continuously and non invasively is of great importance in clinical routine. It can even be necessary to analyse blood perfusion on maps (i.e. two-dimensionally). This has become possible with the LDF technique.

Laser Doppler flowmetry systems can be separated into two categories, namely the laser Doppler perfusion moni-

tors (LDPM) and the laser Doppler perfusion imagers (LDPI). Laser Doppler perfusion monitoring and imaging are easy to use techniques and have supplemented other methods that have been presented in detail in the literature (photoelectric plethysmography, video-photometric capillaroscopy, thermal and radioisotope clearance, orthogonal polarization spectral imaging). Clinical applications of the laser Doppler technique are related to diabetes microangiopathy, peripheral vascular diseases, Raynaud's phenomenon, pharmacological applications, thermal injury, plastic surgery, flap surveillance, skin diseases, ... [2, 40, 49, 50, 58]. However, useful results can only be obtained with an understanding of the technique principles, the knowledge of its limitations, and an accurate processing of the signals. Mixing engineering and medicine fields is indispensable in this way. This can be achieved, among others, by proposing modelling of the underlying mechanisms, by improving the knowledge of the physiological activities acting at the microcirculation level and by the process of the recordings given by clinicians.

This paper aims at offering the state-of-the-art on the laser Doppler perfusion technique. After a review of the theory giving rise to the perfusion signal, it will be dedicated to the benefits brought by signal processing methods applied on LDF recordings. Afterwards, novel approaches in velocity components and imaging will be presented. Finally, future trends and concluding remarks will be given.

2 Theory of laser Doppler flowmetry

2.1 Introduction

The laser Doppler perfusion monitoring and imaging techniques rely on the Doppler effect, first described by the Austrian scientist Johan Christian Doppler [57]. In 1972, Riva et al. were the first ones to report microvascular blood flow measurements with the Doppler effect [52]. Stern then suggested that tissue perfusion, as opposed to flow in a single vessel, could be measured with the LDF technique [61]. These works were followed by several studies that have been carried out to improve the technique and the measurements; the theory has also been established [3, 11, 22, 23, 29, 41, 42, 44, 45, 53, 61, 62].

The most common way to design a laser Doppler flowmeter is by using a fibre optic probe (generally 0.25 mm between the transmitting and receiving fibres). This leads to a sampling depth on the order of 1 mm for human skin [4, 38]. When coherent light is directed toward a tissue, photons are scattered by moving objects and by static structures. If they encounter moving particles, the Doppler effect appears. The photon frequency is therefore modified. When the reemitted light is directed toward a photodetector, optical mixing of light frequency shifted and non frequency shifted gives rise to a stochastic photocurrent. The power spectrum $P(\omega)$ of this photocurrent is linked to the blood cells properties present in the illuminated volume. More precisely, when the concentration of moving red blood cells is low, the first moment $\int \omega P(\omega)\,\mathrm{d}\omega$ scales with the concentration of moving blood cells (CMBC) times their average velocity, whereas $\int P(\omega)\,\mathrm{d}\omega$ scales with the CMBC [48].

It is convenient to view light as a particle with some wave characteristics, in describing quasi-elastic light scattering [43]. The Doppler effect results in a spectral broadening of light, due to interactions with moving scatterers, mainly red blood cells (RBCs). The blood cells are moving at low velocities, on the order of millimeters per second, in the microcirculation, giving rise to minute frequency shifts, about 10^{-11} times smaller than the frequency of the incident light [49]. Consequently, it is critical that the light source is highly monochromatic (i.e. temporally coherent). This is what makes the laser an ideal light source for the quasi-elastic light scattering applications [57]. Even though other authors presented models earlier, most of the theories are based on the work by Bonner and Nossal [3]. Several variations on these theories have subsequently been presented [1, 4, 5, 47]. The following derivations are based on the work by Nilsson et al. [47], unless otherwise stated, and are taken from the PhD thesis of Nilsson [43]. A recent derivation can also be found in reference [48].

2.2 Model validity

The subsequent theoretical framework of the microvascular blood perfusion estimate, obtained using the LDF method, is based on the following assumptions:

1. Light suffers multiple scattering in the static tissue matrix, hence becoming diffusely scattered.
2. The fraction of photons undergoing multiple Doppler shifts is negligible.
3. The blood cell velocities are randomly distributed in direction within the scattering volume, meaning that the network of microvessels, in effect, is random on a length scale defined by the mean distance between RBC scattering events.
4. The statistics of the blood cell velocity field is uniform throughout the scattering volume.
5. Statistical parameters are stationary throughout the signal sampling phase (for the Fourier transform to be valid).

Some of these assumptions may not be valid in real tissue; in fact, only 1. can be considered completely true, and the other assumptions may be more or less incorrect. Nevertheless, the following theory results in measurable

quantities which have been verified to agree well with theoretical predictions in multiple flow models [47].

2.3 Single scattering event

The incident photon, as seen from the moving blood cell, can be described by the electric field vector, $\mathbf{E}_{\text{in}}$, [47]

$$\mathbf{E}_{\text{in}} = E_{0i}\mathrm{e}^{i(\omega t - \mathbf{k}_1(\mathbf{v}t + \mathbf{r}_0))}, \tag{1}$$

where E_{0i} is the amplitude, ω the angular frequency and $\mathbf{k}_1$ the wave vector of the incident light (Fig. 1). $|k_a| = 2\pi/\lambda_t = 2\pi\ n/\lambda_{\text{vacuum}}$, λ_t = wavelength of the light in the medium with refractive index n. $r = \mathbf{v}t + \mathbf{r}_0$ describes the present position of the photon. Consequently, the scattered photon can be described by the scattered electric field vector, $\mathbf{E}_{\text{sc}}$ [47],

$$\mathbf{E}_{\text{sc}} = E_{0s}\mathrm{e}^{i(\omega t - \mathbf{k}_1(\mathbf{v}t + \mathbf{r}_0)) + i\mathbf{k}_2\mathbf{v}t}, \tag{2}$$

where E_{0s} represents the amplitude and $\mathbf{k}_2$ the wave vector of the scattered light. After rearrangement, $\mathbf{E}_{\text{sc}}$ can be written on the form

$$\mathbf{E}_{\text{sc}} = E_{0s}\mathrm{e}^{i\omega t}\mathrm{e}^{-i\varphi}\mathrm{e}^{-i\mathbf{q}\mathbf{v}t}, \tag{3}$$

since the Bragg scattering vector, $\mathbf{q} = \mathbf{k}_1 - \mathbf{k}_2$, and $\phi = \mathbf{k}_1\ \mathbf{r}_0$ are time-invariant phase constants. Thus, the scattered photon is described by the incident, carrier frequency, ω, a time-invariant phase constant, ϕ, and a time-varying phase factor, $\mathbf{q}\mathbf{v}t$, which describes the angular Doppler frequency, $\omega_{\text{D}} = \mathbf{q}\cdot\ \mathbf{v}$.

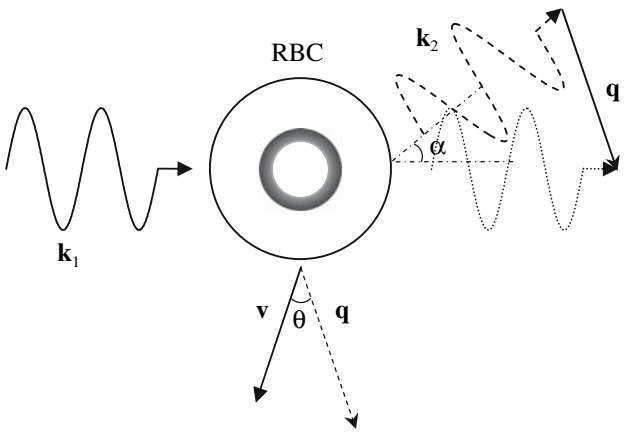

Fig. 1 Single scattering event between a photon and a moving scatterer, in this case a red blood cell (*RBC*). $\mathbf{k}_1$ and $\mathbf{k}_2$ denote the incoming and scattered wave vectors, and α is the angle between the two. $\mathbf{v}$ is the velocity vector of the RBC. $\mathbf{q}$ is the Bragg scattering vector. θ is the angle between $\mathbf{q}$ and $\mathbf{v}$ (Figure from Nilsson PhD thesis [43], reproduced with the kind permission of Nilsson)

2.4 Photocurrent and intensity autocorrelation function

Now, the infinitesimal photocurrent at time t, $i(t,\mathbf{r})$, on the detector surface, at $\mathbf{r}$, produced by the total scattered electric field, $\mathbf{E}_{\text{T}}$, is

$$i(t,\mathbf{r}) = C_0[\mathbf{E}_{\text{T}}(t,\mathbf{r})\mathbf{E}^*_{\text{T}}(t,\mathbf{r})], \tag{4}$$

where C_0 is an instrumentation constant, $\mathbf{E}_{\text{T}}$ is the sum of the electric fields originating from scattering in moving and static structures, and $\mathbf{E}^*_{\text{T}}$ is the complex conjugate of $\mathbf{E}_{\text{T}}$ [47]. Integrating $i(t,\ \mathbf{r})$ over the entire photosensitive detector area results in the total photocurrent, $i(t)$,

$$i(t) = \int\limits_{\substack{\text{detector}\\ \text{area}}} i(t,r)\,\mathrm{d}^2r. \tag{5}$$

It has been shown that, disregarding of noise and the heterodyne efficiency, the ACF of the photocurrent, or intensity, in one coherence area, may in a simplified form be expressed as [47; personal communication]

$$\begin{aligned}\text{ACF} = \langle i(0)i(\tau)\rangle &= \left\langle \mathbf{E}_{\text{T}}(0)\mathbf{E}^*_{\text{T}}(0)\mathbf{E}_{\text{T}}(\tau)E^*_{\text{T}}(\tau)\right\rangle \\ &= 2i_R\langle i_S\rangle + i_R^2 + \langle i_S\rangle^2 + i_R\langle i_S\rangle\left(\left\langle \mathrm{e}^{i\mathbf{q}\mathbf{v}\tau}\right\rangle\left\langle \mathrm{e}^{-i\mathbf{q}\mathbf{v}\tau}\right\rangle\right) \\ &\quad + \langle i_S\rangle^2\left\langle \sum_{m=1,m\neq n}^{S}\sum_{n=1}^{S}\mathrm{e}^{i(\mathbf{q}_m v_m - \mathbf{q}_n v_n)\tau}\right\rangle,\end{aligned} \tag{6}$$

where the ACF is a measure of how much the signal resembles itself at two different points in time ($t = 0$, and $t = \tau$, respectively), calculated as an ensemble average (Eq. 7) over an ''infinite'' time. $i_S = SE^2_{0S}$ is the current produced by photons scattered in moving structures, and S is the number of photon interactions with moving structures, contributing to the total electric field. Similarly, $i_R = RE^2_{0\text{R}}$ for interactions with static structures. In the above equation, the first three terms constitute the time invariant, or DC signal. The fourth term has contributions both from photons scattered in static and moving structures, i.e. heterodyne mixing. The fifth term is made up of light scattered by moving structures, mixed with itself (homodyne mixing), and can be neglected in the subsequent calculations, because of assumption 2 in Sect. 2.2.

2.5 Relation between the single scattering event and the intensity ACF

First, we need to define the ensemble average, or expectation value of a function $g(x)$, $\langle g(x)\ \rangle$,

$$\langle g(x)\rangle = \int g(x)f(x)\,\mathrm{d}x, \tag{7}$$

where $f(x)$ is a probability density function of x. Hence, for a fixed value of q, the ensemble average of the time-varying phase factor in Eq. 3 can be described as

$$\left\langle e^{-i\boldsymbol{q}\boldsymbol{v}\tau}\right\rangle_{\boldsymbol{v}} = \underbrace{\iiint}_{\substack{\text{velocity}\\ \text{field}}} N_0(\boldsymbol{v}) e^{-i\boldsymbol{q}\boldsymbol{v}\tau} d^3\boldsymbol{v}, \tag{8}$$

$N_0(\boldsymbol{v})$ is the normalized three dimensional velocity distribution, determining the relative number of RBCs moving with velocity $\boldsymbol{v}$. Assumption 3 in Sect. 2.2 ascertains that $N_0(\boldsymbol{v})$ is independent of the spatial coordinates. Making $\boldsymbol{q}$ parallel to the z-axis, and transforming the integral to spherical coordinates results in [47, personal communication]

$$\left\langle e^{-i\boldsymbol{q}\boldsymbol{v}\tau}\right\rangle_{v} = \int_{v=0}^{\infty} N(v)\frac{\sin(qv\tau)}{qv\tau}\mathrm{d}v, \tag{9}$$

where the one dimensional velocity distribution $N(v) = 4\pi v^2 N_0(v)$; thus, there is no preferential direction of the moving scatterers, but merely a speed distribution. Introducing a scattering vector distribution, $S_0(\mathrm{q}(\alpha))$, it is possible to derive an expression for the one dimensional scattering vector distribution, $S(q(\alpha))$, taking into account the three dimensional nature of the scattering event in Fig. 2, and assuming azimuthal symmetry around $\mathbf{k}_1$. Letting $|\mathbf{k}^2| = r$, and the area of the infinitesimally thin ring be A_r. Then dividing A_r by the total area of the sphere surface for all three dimensional scattering angles, A_s, the one dimensional transformation factor is derived, and can be written as

$$\frac{A_r}{A_s} = \frac{2\pi(r\sin(\alpha))(r\sin(d\alpha))}{4\pi r^2} \approx \frac{1}{2}\sin(\alpha)\,\mathrm{d}\alpha. \tag{10}$$

Therefore, the expectation value of the time-dependent phase factor, $\langle e^{-i\boldsymbol{q}\boldsymbol{v}}\,\tau\rangle_{\boldsymbol{v}}$, over the entire $\mathbf{q}$-vector field may be written as [47]

$$\left\langle\left\langle e^{-i\tau}\right\rangle\right\rangle = \int_{v=0}^{\infty} N(v)\int_{\alpha=0}^{\pi}\frac{\sin(qv\tau)}{qv\tau}S(q(\alpha))\frac{1}{2}\sin(\alpha)\mathrm{d}\alpha\mathrm{d}v, \tag{11}$$

hence relating the one dimensional RBC velocity, $N(v)$, and scattering vector, $S(q(\alpha))$, distributions to the measurable intensity ACF, produced by the heterodyne mixing term of Eq. 6 (term four).

2.6 Photocurrent power spectrum

According to the Wiener–Khintchine theorem, the photocurrent power spectrum, $P(\omega)$, produced by the heterodyne mixing term in a single coherence area, is the Fourier transform of the intensity ACF, disregarding homodyne mixing [4]. According to Nilsson et al. [47, personal communication]

$$P(\omega) \propto i_R^2\langle i_S\rangle \int_{v=0}^{\infty} N(v)\int_{\alpha=0}^{\pi}\sin(\alpha)S(q(\alpha)) \times \int_{\tau=-\infty}^{\infty}\frac{\sin(qv\tau)}{qv\tau}e^{i\omega\tau}\mathrm{d}\tau\,\mathrm{d}\alpha\,\mathrm{d}v. \tag{12}$$

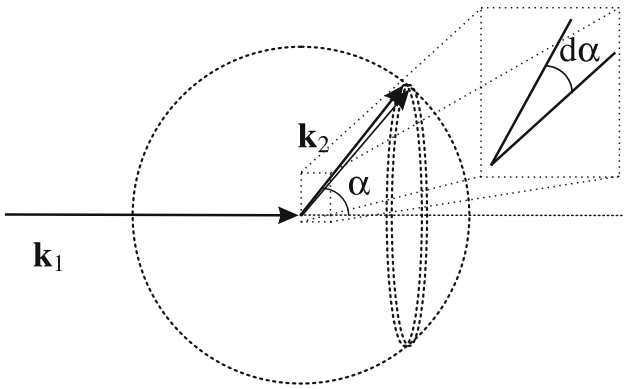

Fig. 2 Schematic to show three dimensional scattering of light due to a RBC (not shown in the figure, but located at the origin). $|\mathbf{k}_2|\sin(\mathrm{d}\alpha)$ corresponds to the thickness of an infinitesimally thin ring, with radius $|\mathbf{k}_2|\sin(\alpha)$, that represents the exiting angle, α, of the scattered photon. Azimuthal symmetry is assumed around $\mathbf{k}_1$ (Figure from Nilsson PhD thesis [43], reproduced with the kind permission of Nilsson)

2.7 Deriving the perfusion estimate

Equation 12 can be rewritten, assuming $|\mathbf{k}_1| \approx |\mathbf{k}_2| = \mathbf{k} = 2\pi/\lambda_t$, where the laser wavelength in the tissue can be written as $\lambda_t = \lambda_{\text{vacuum}}/n_t$, n_t representing the refractive index of the tissue. The angular Doppler frequency, ω_{D}, is expressed as $\omega_{\mathrm{D}} = \mathbf{q}\cdot\mathbf{v} = |\mathbf{q}|\,|\mathbf{v}|\cos(\theta)$. According to the cosine theorem,

$$\omega_D = \frac{4\pi}{\lambda_t}\sin\left(\frac{1}{2}\alpha\right)v\cos(\theta) \tag{13}$$

where $\mathbf{v} = |\mathbf{v}|$. After normalization with the total light intensity, Nilsson et al. [47] have shown that

$$\mathrm{CMBC} \propto \int_0^{\infty} P(\omega)\,\mathrm{d}\omega \propto \int_{v=0}^{v_{\max}}\langle i_S\rangle N(v) \times \int_{x=0}^{\frac{4\pi}{\lambda_t}} x\int_{q=x}^{\frac{4\pi}{\lambda_t}} S(q)\mathrm{d}q\,\mathrm{d}x\,\mathrm{d}v, \tag{14}$$

$$\text{Perfusion} \propto \int_0^{\infty} \omega P(\omega)\,\mathrm{d}\omega \propto \int_{v=0}^{v_{\max}} \langle i_S \rangle v N(v) \times \int_{x=0}^{\frac{4\pi}{\lambda_t}} x \int_{q=x}^{\frac{4\pi}{\lambda_t}} S(q)\mathrm{d}q\,\mathrm{d}x\,\mathrm{d}v \tag{15}$$

Consequently, the outer integral in Eq. 14 scales linearly with $\langle i_S \rangle$, which is linearly related to the number of moving RBCs in the scattering volume, if assumption 2 of Sect. 2.2 is valid. The two inner integrals are independent of v. Therefore, the integral of $P(\omega)$, i.e. the area under the power spectral density curve, is also referred to as the CMBC (Fig. 3a). Similarly, in Eq. 15, the outer integral constitutes a measure of the product of the factor $\langle i_S \rangle$, and the average velocity of the RBCs ($\int vN(v)\,\mathrm{d}v$). This integral of the product of the concentration of moving RBCs and the average velocity, or the ω-weighted power spectral density, is usually denoted the *perfusion estimate* (Fig. 3b).

The perfusion estimate in Eq. 15 carries no information about the direction of flow, because of assumptions 1 and 3 of Sect. 2.2, ensuring that the change in scattering vector, Δq, resulting from a collision of a photon with a RBC, will be uncorrelated with the direction in which the cell is moving [4]. Accordingly, the directional information that is present, e.g. in the case of Doppler ultrasound, is lost due to the diffuse scattering of light in the tissue surrounding the microcirculation. Sound, on the other hand, essentially moves on a straight path through tissue, and a small fraction is reflected off the moving RBCs in larger vessels, returning to the detector. The Doppler frequency shift is inversely related to the wavelength of the incoming sound, or light (Eq. 13). Since the wavelength of visible light is approximately 500 times smaller than that of ultrasound, the corresponding frequency shifts will be 500 times greater. This is the principal reason why capillary flow rates of about 1 mm/s cannot be resolved using conventional Doppler ultrasound, since the frequency shifts produced are immeasurably small (about 5 Hz) [4].

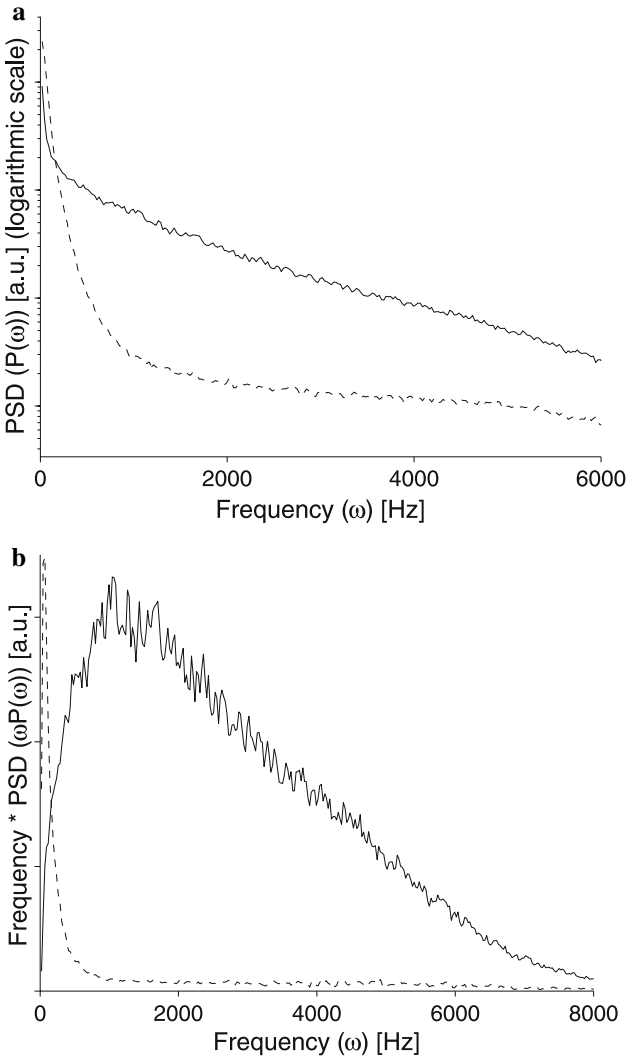

Fig. 3 **a** *Top* power spectral density (PSD), $P(\omega)$ versus ω measured on volar forearm skin (*dashed line*) and fingertip (*solid line*). Note that the power is contained at higher frequencies in the case of the fingertip, indicating higher RBC velocities and/or multiple Doppler shifts. **b** *Bottom* ω-weighted power spectrum, enhancing the importance of the higher frequency components in the contribution to the final perfusion estimate. Note the difference in scale on the x axis, and the logarithmic y axis in **a**. After proper calibration, normalization and linearization, the perfusion estimate was calculated to be approximately 21 times greater in the fingertip, compared to the forearm skin, in this particular case (Figure from Nilsson PhD thesis [43], reproduced with the kind permission of H. Nilsson)

3 Signal processing benefits

3.1 Introduction

The perfusion estimate according to Eq. 15, when measurements are made in vivo, will exhibit oscillations due to, among others, microvascular processes such as myogenic, neurogenic and endothelial related metabolic activities. The knowledge of these processes' contribution in several situations could bring information that would help in understanding pathologies. That is why oscillatory components of LDF signals have recently been deeply investigated [7, 8, 33, 35, 36, 59, 60]. The three above-mentioned activities can now be studied from LDF time–frequency representations obtained with wavelets. Quantitative measures were also introduced to determine their contribution.

Studies carried out with scalograms (square modulus of the wavelet transform) on LDF signals recorded on humans

have shown that five peaks arise, respectively around 1, 0.3, 0.1, 0.04 and 0.01 Hz. In addition to the heart beats and the respiration (whose activity gives the peaks around 1 and 0.3 Hz respectively), the myogenic activity (the smooth-muscle cells in the vessel walls respond continuously to the changes in intravascular pressure) gives rise to oscillations with a frequency around 0.1 Hz. The peak around 0.04 Hz results from the neurogenic activity. Eventually, oscillations with a frequency around 0.01 Hz are thought to correspond to the endothelial related metabolic activity [60]. Moreover, a very recent study has also hypothesized that other endothelial mechanisms such as endothelium-derived hyperpolarizing factor (EDHF) might be involved in the regulation of a sixth frequency interval (0.005–0.0095 Hz) [32].

An application of these results has been dedicated to the study of the vasodilation that appears on healthy subjects when a local and progressive pressure is applied on skin (see below). The limited amplitude of this phenomenon on type 1 diabetic patients could explain the development of decubitus ulcers on such patients. Moreover, other reversible perturbations such as physical exercises, application of vasoactive substances... were investigated too [21, 34, 66]. Irreversible perturbations resulting from ageing or diseases were also analysed (diabetes, heart failure, acute myocardial infarction) [6, 65]. The results of these signal processings show that the oscillatory components in LDF signals have strong physiological and clinical implications.

3.2 Example of the use of signal processing tools: understanding the microvascular perfusion signals during the application of a low and progressive pressure

3.2.1 The pressure-induced vasodilation phenomenon

Local pressure strains to the skin appear to be those of the major determinants of cutaneous lesions in multiple clinical situations (pressure wounds, diabetic foot ulcers...). At the end of the 1990s, Fromy et al. [17] reported an original nervous reflex of skin vasodilation mediated by primary afferent fibres. This phenomenon has been observed in healthy rats as well as in healthy human subjects (Figs. 4 and 5a). The vasodilatory response disappears when pretreatment with a local anaesthetic is applied [17]. This pressure-induced vasodilation (PIV) response is a transient adaptive phenomenon acting as a protective mechanism without which certain pressure-associated lesions may develop. In absence of PIV, skin blood flow is progressively decreased with application of increased pressures. However, diabetic patients may present skin blood flow responses to locally applied pressures different from the ones observed on healthy subjects (see Fig. 5b) [20, 31]. The differences could, in part, explain the development of decubitus and plantar ulcers.

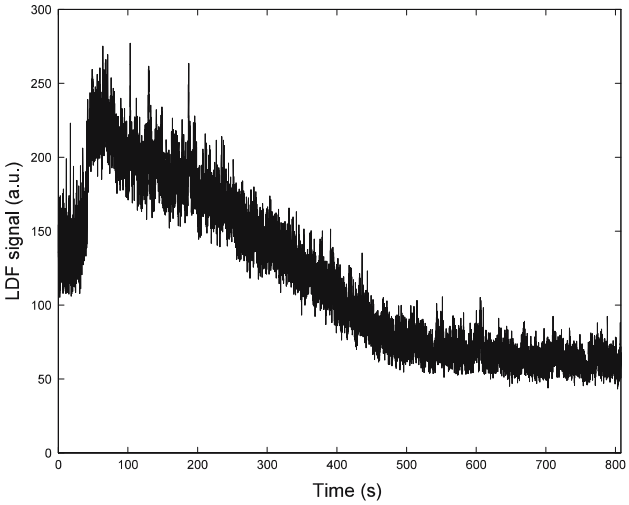

Fig. 4 Cutaneous pressure-induced vasodilation signal obtained on an anaesthetised rat. Time $t = 0$ represents the beginning of the increasing pressure application (11.1 Pa/s) (Figure reprinted from Fig. 1 in Ref. [24] Copyright (2006) with permission from SPIE)

The studies carried out to know the mechanisms implied in PIV have shown that PIV depends on capsaicin-sensitive fibres in rats and in humans [17, 18]. It has also been shown that calcitonin-gene-related peptide (CGRP) plays a major role in the development of the response, whereas neurokinins have no role. Moreover, endothelial nitric oxide (NO) is crucial in PIV development. Prostaglandins and neuronal NO are also involved [18]. Recently, further studies using signal processing techniques have been carried out to improve the PIV knowledge [24–27]. Their goal was, among others, to explain the differences observed in the responses of healthy and diabetic subjects.

3.2.2 Time-frequency analyses to determine the activities implied in PIV[1]

As mentioned previously, a scalogram analysis of LDF signals provides information dealing with the myogenic, neurogenic and endothelial activities behaviour. Therefore, in order to have a precise knowledge of these activities at rest and during the application of a local and progressive pressure, on healthy and type 1 diabetic subjects, a study analysed LDF signals recorded at rest and during the application of a progressive pressure, on six diabetic patients with type 1 diabetes mellitus and without respiratory or cardiac failure, neuropathy of nondiabetic origin, peripheral vascular disease, psychological disorder or tremor, and on six age-matched non-diabetic control subjects

[1] A detailed description of the work presented in this paragraph can be found in Ref. [26].

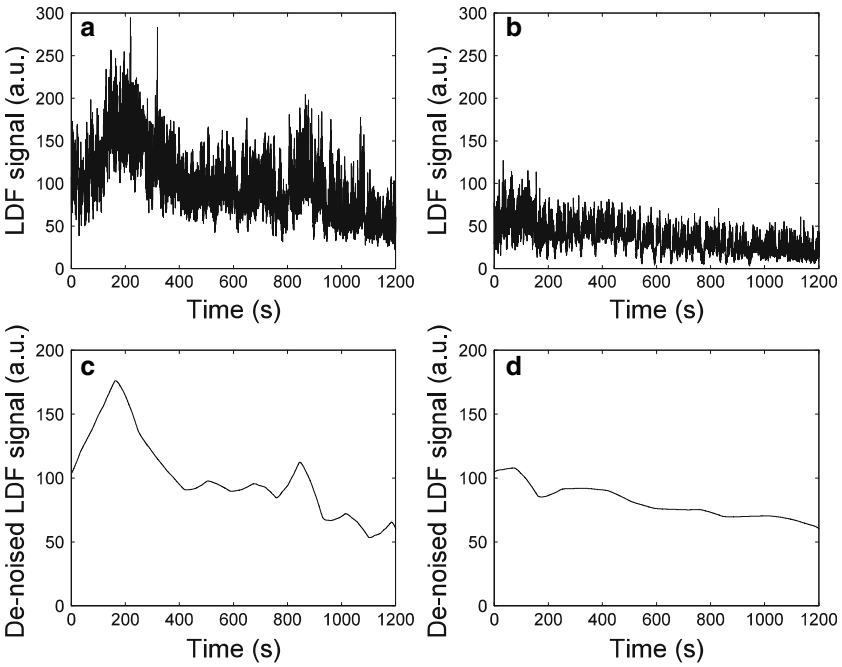

Fig. 5 **a** Original LDF signal recorded on a healthy subject in a quiet temperature climatised room (29.5 ± 0.2°C), during a local and progressive cutaneous pressure application (11.1 Pa/s). Time $t = 0$ corresponds to the beginning of the increasing pressure (Figure reprinted from Fig. 1 in Ref. [27] Copyright (2006) with permission from SPIE). **b** Original LDF signal recorded on a diabetic patient in a quiet temperature climatised room (29.5 ± 0.2°C), during a local and progressive cutaneous pressure application (11.1 Pa/s). Time $t = 0$ corresponds to the beginning of the increasing pressure (Figure reprinted from Fig. 2 in Ref. [27] Copyright (2006) with permission from SPIE). **c** De-noised normalised version of the signal presented on Figure 5a (Figure reprinted from Fig. 3 in Ref. [27] Copyright (2006) with permission from SPIE). **d** De-noised normalised version of the signal presented on Fig. 5b (Figure reprinted from Fig. 4 in Ref. [27] Copyright (2006) with permission from SPIE)

[26]. Based on other studies [19, 25, 28], the scalograms of each signal were then studied between 0.0095 and 0.145 Hz, in order to obtain the three characteristic frequencies corresponding to the myogenic, neurogenic, and endothelial related metabolic activities: intervals 0.052–0.145, 0.021–0.052, 0.0095–0.021 Hz, respectively [26]. Quantitative measures were then calculated to make comparisons between sets of recordings: the energy of the time–frequency representation on a given frequency band [25, 26], and the relative energy of the time-frequency representation on a frequency band [26]. To have frequency analyses during the time variations of the signals recorded during the local and progressive cutaneous pressure application, these quantities were calculated on the whole recordings (that lasted 16 min 40 s), but also on signal segments of 200 s length.

For the analysis, four kinds of comparisons were performed, as mentioned on Fig. 6. At first, the quantitative measures were statistically analysed between signals recorded at rest on healthy and type 1 diabetic subjects. Then, the quantitative measures were statistically analysed between signals recorded simultaneously at rest and during the progressive pressure application on healthy subjects. Afterwards, the latter statistical analysis was performed on diabetic patients. Eventually, the quantitative measures were compared between signals recorded during the progressive pressure application on healthy and diabetic subjects. A schematic representation of the whole process providing the results is shown on Fig. 6.

The Wilcoxon matched pairs test was used to evaluate the differences of the blood flow dynamic properties between signals recorded simultaneously (at rest on one site and during the progressive pressure application on the other) on healthy and diabetic subjects (second and third comparisons mentioned above). The Mann–Whitney test was used to evaluate the differences of the blood flow dynamic properties between the two groups of subjects (first and fourth comparisons mentioned above). Statistical significant differences were defined as $P < 0.05$.

The results [26] showed that, at rest, the scalogram energy of each frequency band studied is significantly lower for diabetic patients than for healthy subjects, but the scalogram relative energies do not show any statistical difference between the two groups of subjects. Moreover, the relative contribution of the endothelial related metabolic activity is significantly higher during the application of a progressive pressure than at rest, in the interval 200–400 s following the beginning of the increasing pressure

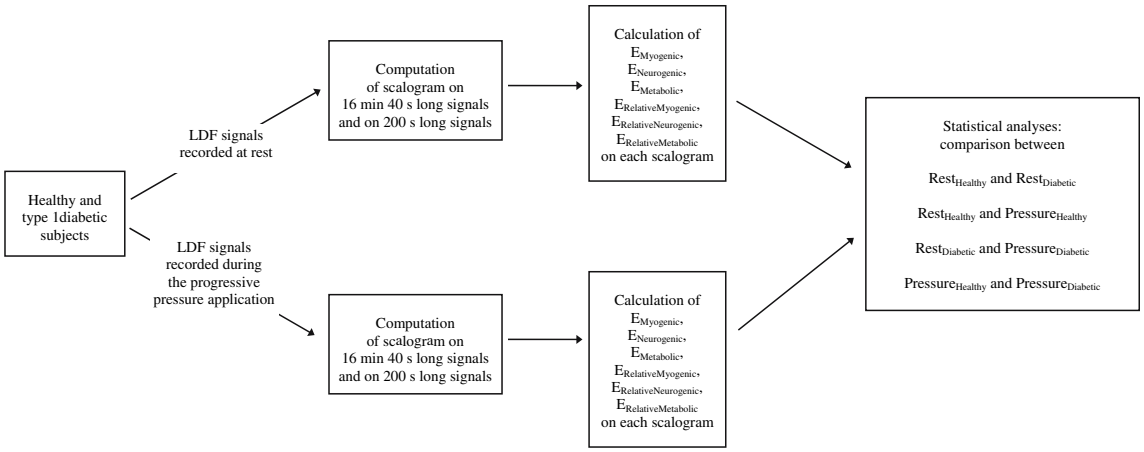

Fig. 6 Schematic representation of the LDF signal process used (Figure modified from [26], reproduced with the kind permission of IOP Publishing Limited)

application, but only for healthy subjects. The results obtained lead to interesting results in order to improve the knowledge on cutaneous microvascular responses to injuries or local pressures initiating diabetic complications. This signal processing work, together with the pharmacological analyses [18], therefore brings some explanations on the early decrease of skin blood flow observed at low applied pressures in diabetic patients. These approaches, based on the present knowledge, have now to go further in order to prevent the formation of cutaneous lesions generated by pressure applications.

3.2.3 *Wavelet de-noising to determine the dynamic characteristic of PIV signals*[2]

In order to increase the understanding of LDF signals observed on healthy and type 1 diabetic subjects during the application of a local and progressive pressure, the dynamic characteristics of the recordings were also studied. The dynamic characteristics refer to the time to reach the peak of perfusion, time called *tpLDF* (time $t = 0$ at the beginning of the increasing pressure application), the perfusion maximum value reached at *tpLDF*, perfusion value called *pLDF*, and the value of the perfusion reached at the end of the experiment, called *vZero* (value computed as the mean value of the de-noised normalised signal between 17 and 20 min following the beginning of the increasing pressure application) [27]. Nevertheless, LDF signals present oscillations (see above) that prevent an easy computation of the signal dynamic characteristics. Some authors therefore proposed to de-noise, with wavelets, the signals recorded on healthy and type 1 diabetic subjects [24, 27].

For that purpose, six diabetic patients with type 1 diabetes mellitus and six age-matched non-diabetic control subjects were studied [27]. Data collection began with a 2-min control period before the onset of pressure increase (11.1 Pa/s rate of pressure increase). Cutaneous blood flow was then continuously recorded for 22 min. A wavelet de-noising algorithm was then applied on each recording. The method of de-noising proposed by the authors uses only the approximation coefficients to reconstruct the signals [27]. The details, i.e. the high-frequency components, are removed. Another work [51] noted that the ''near symmetric wavelet'' with four vanishing moments (''sym4'' wavelet) achieves a good compromise between noise reduction and over-smoothing. To process the human LDF signals the latter wavelet was therefore chosen. Once the 12 LDF signals were de-noised, each one was normalised to 100 a.u. The dynamic characteristics were then computed on each de-noised normalised signal.

The wavelet-based algorithm applied to LDF signals recorded during a local and progressive cutaneous pressure application, on healthy and type 1 diabetic subjects, gives noise-free signals (see Fig. 5c, d). The dynamic characteristics can therefore be obtained accurately. The results are mentioned in Table 1 [27]. The values show that a large vasodilation exists on healthy subjects. The mean peak of perfusion occurs at 3.2 kPa approximately. However, a vasodilation of limited amplitude appears on diabetic patients. For them, the highest perfusion value is visualised, on the average, at 1.1 kPa. The differences could, in part, explain the development of decubitus and plantar ulcers. The LDF technique therefore allows, after a signal processing work based on wavelets, an accurate determination of the dynamic characteristics of this reflex that could prevent ischemia in healthy people.

[2] A detailed description of the work presented in this paragraph can be found in Ref. [27].

Table 1 Mean values of the dynamic characteristics computed on the de-noised normalised signals (Table reprinted from Table 1 in Ref. [27] Copyright (2006) with permission from SPIE)

	Healthy subjects	Diabetic patients
tpLDF (s)	287.5	100.3
pLDF (a.u.)	182.3	131.6
vZero (a.u.)	64.9	71.9

4 Novel approaches in velocity components and perfusion imaging

4.1 Novel approaches in velocity components

4.1.1 Background

As mentioned previously, the microcirculatory network, the most peripheral part of the circulatory system, includes arterioles, metarterioles, capillaries, arteriovenous anastomosis and venules. Through this network nutrients and waste products are delivered to and from the tissues. In LDF, the microcirculatory perfusion is defined as the concentration of moving RBCs times their average velocity $\langle v \rangle$. Coherent laser light, injected into the tissue, is scattered by static tissue and by moving RBCs, the latter causing a Doppler shift that can be described by the single scattering event (defined in the previous Theory part of the paper). Optical mixing of unshifted and frequency shifted light on a photodetector, causes a time varying photocurrent with statistical properties that reflects the perfusion. By analyzing the power spectrum of the photocurrent, $P(\omega)$, it can be shown that

$$\int \omega^n P(\omega)\,\mathrm{d}\omega \propto \mathrm{CMBC}\langle v^n \rangle \tag{16}$$

A measure of CMBC is obtained for $n = 0$ and perfusion, as defined above, for $n = 1$. Among the assumptions are a low CMBC and a velocity distribution that is independent of the spatial coordinates [48]. A low and homogenously distributed CMBC implies that homodyne optical mixing of Doppler photons (self-mixing of Doppler shifted photons) and multiple Doppler shifts can be neglected. If, however, the CMBC is too high nonlinearities arise. An empirical compensation method has been developed by Nilsson [42], which is valid for the spatial distribution of RBCs in his flow model.

4.1.2 Theory

The method for LDF photocurrent power spectrum analysis proposed by Larsson and Strömberg is derived from frequency domain calculations based on the optical spectrum [37]. A set of reference Doppler spectra are calculated and used in a decomposition algorithm. The reference spectra are calculated using the Monte Carlo method for representative flow velocity regions, assuming an even distribution of particles with a parabolic flow profile. For each velocity component, a single shifted optical Doppler spectrum was calculated using a fast and simple Monte Carlo algorithm, assuming an isotropic distribution of the angle between the incident photon and the scattering particle [37]. Furthermore, the velocity of each particle was randomly chosen between zero and twice the mean velocity of the particles, mimicking a parabolic flow profile. As scattering phase function, the two-parametric Gegenbauer kernel phase function, was used [16, 37]. A recorded LDF spectrum, in general originating from photons that are multiple Doppler shifted to some degree, is decomposed into those velocity regions. This is done by fitting the measured spectrum to a combination of reference spectra, each representing a velocity region. If the measured spectrum is a single Doppler scattering spectrum (low CMBC and no multiple Doppler shifts), the decomposition can be done by linear least-squares fitting [37]. In the extended method [16] incorporating multiple Doppler shifts and homodyne mixing, Monte Carlo simulations have a key role for estimating the degree of shifted photons and the distribution of multiple Doppler shifts. This requires knowledge of the geometry and optical properties of the flow model (or tissue). Both methods require knowledge of the scattering properties of the moving RBCs.

The frequency content of the resulting detector current is linked to the optical Doppler spectrum $I(\beta)$ [10, 13] as

$$P(\omega) = q_{ac} I(\beta) * I(\beta), \tag{17}$$

where q_{ac} is an instrumental constant and * denotes the cross correlation. From now on, $P(\omega)$ is referred to as the *Doppler power spectrum*, in contrast to the *optical Doppler spectrum* $I(\beta)$. To discriminate various velocity regions of Doppler power spectra that originate from multiple Doppler shifted photons, a mathematical relationship between such spectra and single shifted optical Doppler reference spectra from specific velocity regions is needed. Generally, the Doppler power spectrum is broadened when the degree of multiple Doppler shifted photons increases. Theoretically, an optical Doppler spectrum shifted n times, $I(n, \beta)$, can mathematically be expressed as the cross correlation of the optical Doppler spectrum shifted n–1 times, and a transfer function, $I'(\beta)$,

$$I(n,\beta) = \begin{cases} \delta(\beta), & n = 0 \\ I(n-1,\beta) * I'(\beta), & n > 0 \end{cases} \tag{18}$$

where $\delta(\beta)$ is the Dirac function [61]. The transfer function is given as the sum of the single shifted optical reference

spectra, $I_{v_i}(\beta)$, times the fraction of shifts caused by an RBC of velocity v_i, c_{v_i};

$$I'(\beta) = \sum_{v_i} c_{v_i} I_{v_i}(\beta). \tag{19}$$

It should be noted that c_{v_i} sum up to 1.0.

The number of times each photon is Doppler shifted follows a probability distribution, p_n. In a homogenous media, assuming equal photon pathlengths, that distribution can be well approximated with a Poisson distribution [54]. For the general case, however, the distribution has to be estimated using Monte Carlo simulations [16]. Given this shift distribution, the final optical Doppler spectrum is calculated as

$$I(\beta) = \sum_{n=0}^{\infty} p_n I(n, \beta). \tag{20}$$

The Doppler power spectrum, based on this optical Doppler spectrum, can then be calculated by

$$P(\omega) = I(\beta) * I(\beta) \tag{21}$$

The computation of these equations is time consuming. In order to increase the computation speed, the calculations can be performed in the Fourier domain [16]. In order to fit the velocity components c_{vi} to the measured spectrum P_{meas}, the non-linear Levenberg–Marquardt method was employed. The χ^2 merit function was

$$\chi^2 = \sum \left(1 - \frac{P_{\text{calc}}}{P_{\text{meas}}}\right)^2 \tag{22}$$

where P_{calc} is the calculated multiple shifted Doppler spectrum for the components c_{vi} in each iteration.

4.1.3 Measurements and results

The measurements were performed with a modified Periflux 5000 system (Perimed AB, Järfälla, Sweden), using a diode laser at 786 nm, and a standard optic probe (Probe 408, Perimed AB, Järfälla, Sweden). The probe consisted of one emitting and one receiving step-index fiber, both having a core diameter of 125 μm and a numerical aperture of 0.37. They were separated 230 μm apart (centre to centre distance) at the probe tip. The system was modified by Perimed AB to give the two output signals, ac_m (time varying signal) and dc_m (total light intensity), where the ac_m signal was amplified and band-pass filtered between 8 and 20 kHz, and the dc_m signal was amplified and low-pass filtered using a cut-off frequency of 32 Hz. Both signals were sampled at 50 kHz using a 12-bit AD-card (DAQpad-6070E, National Instruments Inc.). A more detailed description of the data processing has been presented by Larsson and Strömberg [37].

The flow phantom, shown in Fig. 7, consisted of two polythene tubes wrapped pair wise around a piece of white delrin®, about 20 convolutions in two layers. The inner and outer radiuses of the tubes were 0.25 and 0.50 mm, respectively, and the gaps between the tubes were filled with transparent silicone. Another piece of delrin was placed on top of the tubes in order to make the light more isotropic before the interaction with the flow. The flow in the two tubes could be varied independently.

The scattering coefficients of delrin, tube wall and silicone were approximated to 24, 1.0 and 2.0/mm, respectively, and an absorption coefficient of 0.02/mm, refractive index of 1.47 and anisotropy factor of 0.9 were approximated for all materials. Furthermore, the Henyey–Greenstein phase function was assumed for all materials.

Three velocity components with mean velocity of 3.0, 10 and 18 mm/s were fitted to five measurements having various flow velocities in the two tubes with blood diluted to a concentration of 1 %. The velocity in the five measurements were: (1) 3.0 mm/s in both tubes; (2) 10 mm/s in both tubes; (3) 20 mm/s in both tubes; (4) 3.0 mm/s in tube a and 10 mm/s in tube b; and (5) 3.0 mm/s in tube a and 18 mm/s in tube b. The fitted velocity components are shown in Fig. 8. Note the underestimation of the high velocity components for the measurements with velocities (20, 20), (3, 10) and (3, 18) mm/s in the two tubes, respectively.

4.1.4 Conclusions and future works

The new method for analyzing the microcirculatory perfusion by velocity resolved LDF, determines the relative

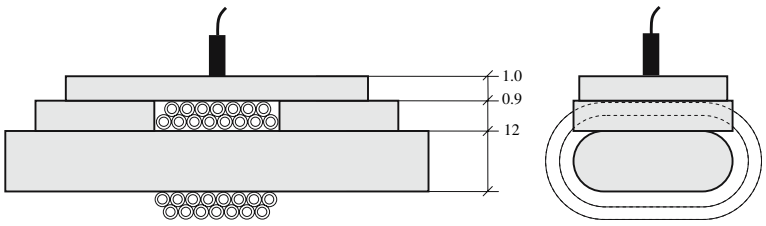

Fig. 7 Flow model (not to scale) with two polythene tubes wrapped pair wise around white delrin® (*gray area*). The two tubes can be perfused independently. Measures are in mm

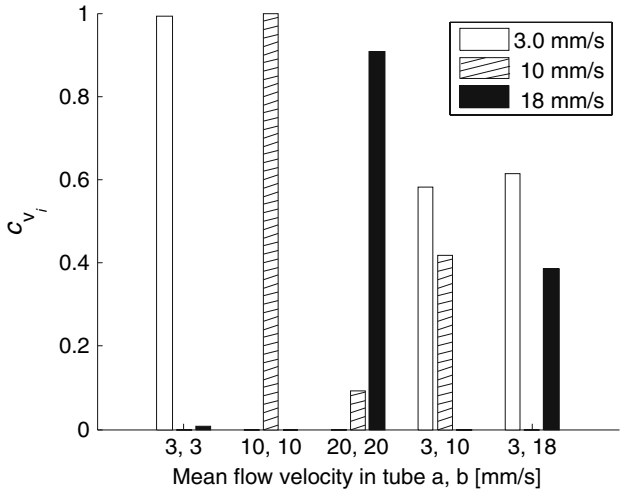

Fig. 8 The three velocity components (c_{vi}), representing mean velocities of 3.0, 10 and 18 mm/s, respectively fitted to five measurements with varying velocity combinations in two tubes in the flow model in Fig. 7

contribution of velocities in physiologically relevant units (mm/s). It has been validated in flow models of single and double tubes perfused with microspheres and blood. Essential in the method is the determination of the degree and distribution of multiple Doppler shifted photons through Monte Carlo simulations. This requires knowledge of the vascular structure of the flow phantom and tissue as well as the optical properties. We are currently developing the method for use in a layered skin model consisting of: *stratum corneum*, *living epidermis*, *papillary dermis*, *upper blood net dermis*, *reticular dermis* and *subcutaneous fat* [39]. The current algorithm is designed to partly handle the inhomogeneity issue as the estimated shift distribution is based on the LDF measure of the concentration of moving scatterers. Still, the effect of physiologically relevant variations in the thickness, the optical properties of the tissue, the blood concentration and the mean blood velocity of each layer has to be determined using Monte Carlo simulations. The relevance of the skin model will be evaluated in vivo using multi channel (multiple fiber separations with different sampling depths) and/or multi wavelength LDF measurements.

4.2 Novel approaches in perfusion imaging

Microvascular blood perfusion is characterised by a great temporal and spatial heterogeneity. Therefore, commonly used laser Doppler flowmeters employing fibre optics sampling a small volume (about 1 mm^3) cannot reflect perfusion differences that appear on adjacent sites. To overcome that problem, LDPI were proposed at the end of the 1980s [12, 46, 67]. For example, LDPI may be of great interest in discriminating between malignant from normal tissues [30, 63, 64].

Current commercial devices use a collimated laser beam which scans the tissue area. The perfusion can be obtained in tissue areas as big as 50×50 cm^2. The most prominent disadvantage of these devices is the time needed to produce a perfusion image, which may be several minutes. This acquisition time is too long to obtain information on certain dynamic processes in the microcirculation. Furthermore, this long acquisition time may cause discomfort for certain patient groups, such as burn victims, young children and elder people. The probability that movement artifacts will degrade the image quality increases with acquisition time. For these reasons efforts are made to reduce the acquisition time and approach the ideal situation of real time whole field perfusion imaging. In these developments, optical imaging arrays play a central role. In addition to fast imaging, devices based on these imaging arrays also render a normal white light photograph of the tissue area. This is often essential for proper interpretation of the perfusion image.

Optical perfusion imaging methods are usually divided into laser Doppler methods and laser speckle methods. These methods are strongly related, since both are based on some analysis of dynamic speckle patterns: time dependent interference patterns formed by interference of a multitude of Doppler shifted coherent waves which are emitted by the tissue. In the methods referred to as 'laser speckle', or 'laser speckle contrast', a tissue area is illuminated by a broad coherent light beam. These methods and their historical development have been described in a review by Briers [9]. The light remitted by the tissue is imaged on an imaging array, with the exposure time chosen such that the speckle pattern is partly blurred due to its dynamic character. The blurring is usually quantified by the mean square or root mean square value of the intensity variations in the blurred speckle pattern, also called the speckle contrast. An alternative quantity is the mean of the absolute value of intensity fluctuations, as used for instance by Forrester [15]. Various methods are encountered in literature to relate the speckle contrast to the motile behavior of particles within the medium under study, such as the particle velocity distribution. However, in many cases the results of a laser speckle contrast measurement are visualized as a spatial distribution of the speckle contrast.

An example of a laser speckle contrast measurement is shown in Fig. 9. These images have been obtained with a CMOS-camera (CCi4, C-Cam Technologies). Here an *ex ovo* chicken embryo and some blood vessels in the chorioallantoic membrane are illuminated with a broad beam of a He–Ne laser (633 nm) with a power of 30 mW. The illumination area is approximately 20×25 mm^2. The speckle contrast has been calculated in 5×5 pixels. Integration

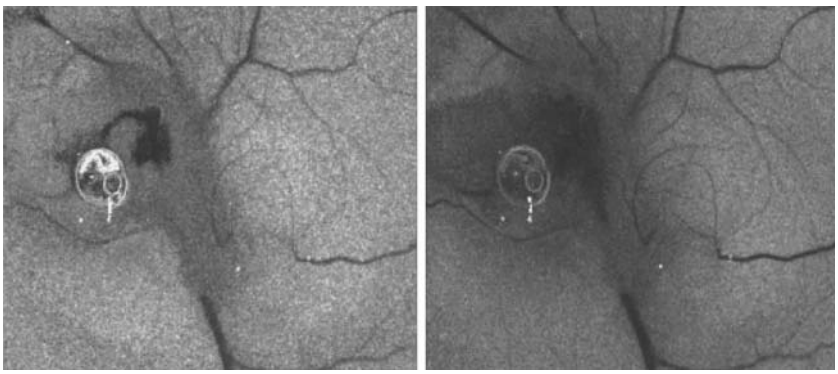

Fig. 9 Speckle contrast distributions in the chicken embryo and the blood vessels in the chorio-allantoic membrane, obtained for camera exposure times of 15 ms (*left*) and 40 ms (*right*). Contrast values were calculated for regions of 5 × 5 pixels

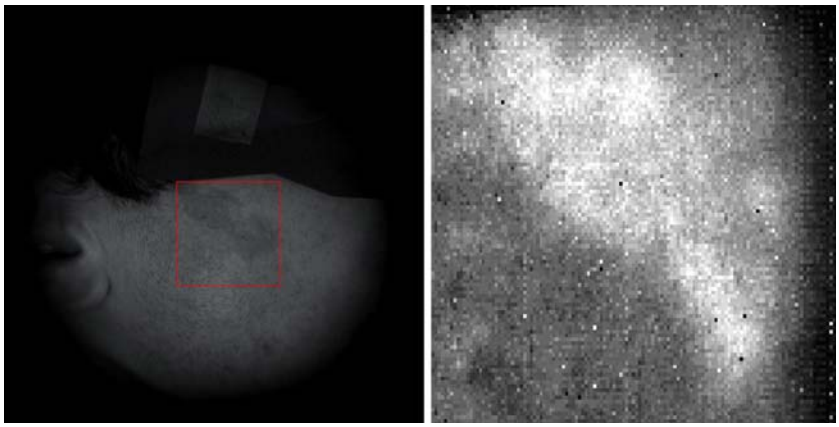

Fig. 10 Photograph (*left*) and laser Doppler perfusion image (*right*) of a pale port wine stain illuminated by a laser beam of size 50 × 50

times were applied of 15 ms (Fig. 9 left) and 40 ms (Fig. 9 right), and only a single exposure was needed. In this case, the speckle contrast has been defined as the intensity-normalized standard deviation of intensity fluctuations, $C = \sigma / \langle I \rangle$. Figure 9 illustrates that visualizations of flow in large and small superficial blood vessels can easily be obtained with the laser speckle contrast principle within a few seconds. While large vessels are visible in both images, the smaller vessels are better represented in the image with the larger integration time, since slow flow causes a slow speckle blurring. While the integration time can be regarded as a free parameter, this also demonstrates a complication of laser speckle contrast methods, since it will not be obvious beforehand which integration time should be chosen. This will depend on flow velocities, but also on signal-to-noise considerations such as shown in Yuan [68].

A more fundamental question with regards to laser speckle contrast methods is the relation of its output to perfusion, and its relation with laser Doppler perfusion imaging. Both methods have been compared mainly empirically [14]. However a comparison based on the fundamental algorithms used in both methods is not available yet. Another issue is that of movement artifacts. In LDPI such artifacts can be suppressed by choice of a proper lower frequency limit in the calculation of spectral moments, while in laser speckle contrast methods no such facility is present.

In LDPI, the step towards real time perfusion monitoring is enabled by the introduction of high speed cameras based on CMOS imaging arrays. In such arrays, the frame rate is inversely proportional to the number of pixels selected. With some of the current commercial cameras, frame rates exceeding 20,000 fps are achievable in pixel regions of sufficient size, such as 128 × 128 pixels. The feasibility of fast LDPI with CMOS cameras has been shown by Serov [55, 56]. An example of a perfusion image obtained with a fast CMOS camera is shown on Fig. 10. A pale port wine stain has been illuminated by a laser beam with a size of 50 × 50 mm^2, a wavelength of 671 nm and a power of 300 mW. Rapid image acquisition has been done in a region of 128 × 128 pixels, at a speed of 27,000 fps. The illuminated area is roughly indicated in the white light photograph of Fig. 10 (left), while Fig. 10 (right) shows the perfusion image, in terms of the first order spectral moment (such as defined by the left-hand side of Eq. 16), normalized by the average intensity. No noise correction has been performed. The perfusion image is extracted from 1,024 raw images. The time needed to produce the perfusion image was approximately 3 s, which is dominated by the time for data transfer and signal processing.

Although no systematic comparison has been performed with a scanning beam LDPI device, it is our impression that the quality of perfusion images in terms of signal-to-noise ratio of scanning beam devices is still better than of camera-based images. An obvious reason for this is the small pixel size of imaging arrays compared to the large photodetectors used in scanning beam devices. Although the fast LDPI devices are in their initial stage of development, now already it would be possible to produce perfusion images at a frame rate of approximately 10 fps, albeit not online but a few seconds after the measurements.

The relative strengths and weaknesses of laser speckle contrast and laser Doppler methods have to be sorted out by careful research. The choice for one or the other method may also depend on the specific requirements in terms of the illuminated tissue area and sensitivity to motion artifacts.

5 Future trends and closing remarks

This paper has reviewed theoretical backgrounds of the laser Doppler flowmetry technique, the benefits, through examples, of signal processing works, as well as novel approaches in velocity components and perfusion imaging. The studies presented in this paper show that signal processing methods (scalograms, wavelet-denoising) are wonderful tools to improve the knowledge of underlying mechanisms detected with the LDF technique. Moreover, a new method for analyzing the microcirculatory perfusion allows the determination, in physiologically relevant units (mm/s), of the relative contribution of velocities. It has been validated in flow models of single and double tubes perfused with microspheres and blood. For the instrumentation part dealing with LDPI, the use of combined light source and CMOS camera has shown to be really interesting in designing new LDPI. Indeed, they provide high speed laser Doppler perfusion imaging on a considerable tissue area, with images available in a few seconds. The same image sensor also provides a photograph, on which the perfusion image can be simply overlayed.

In spite of its recent introduction, the LDF technique has lead to many clinical applications, and new research activities are currently carried out in the clinical and scientific fields. Further work is still needed to improve tools, but also to go further into the interpretation of signals and images. Among these, we can find:

- creation of references in order to have quantitative values
- creation of tools providing a distinction between nutritive (capillary) and global tissue perfusion
- creation of tools providing measurements avoiding motion artefacts.

Acknowledgments The authors would like to thank: Marcus Larsson (PhD) and Ingemar Fredriksson (PhD student). IOP Publishing Limited for their acceptance to reproduce materials from ''Humeau A, Koïtka A, Abraham P, Saumet JL, L'Huillier JP (2004) Spectral components of laser Doppler flowmetry signals recorded in healthy and type 1 diabetic subjects at rest and during a local and progressive cutaneous pressure application: scalogram analyses. Phys Med Biol 49: 3957–3970''. SPIE publication for their acceptance to reproduce materials from ''Humeau A, Koitka A, Saumet J L and L'Huillier JP (2003) Dynamic characteristics of the cutaneous vasodilator response to a local external pressure application detected by the laser Doppler flowmetry technique on anaesthetised rats, in Photon Migration and Diffuse-Light Imaging, David A. Boas, Editor, Proceedings of SPIE-OSA Biomedical Optics, SPIE 5138 72–79'' and from ''Humeau A, Koïtka A, Abraham P, Saumet JL, L'Huillier JP (2004) Dynamic characteristics of laser Doppler flowmetry signals obtained in response to a local and progressive pressure applied on diabetic and healthy subjects, in Photon Management, edited by Frank Wyrowski, Proceedings of SPIE, vol 5456 (SPIE, Bellingham, WA, 2004), pp 307–314''.

References

1. Almond N (1994) Laser Doppler flowmetry: theory and practice. In: Belcaro GV, Hoffman U, Bollinger A, Nicolaides AN (eds) Laser Doppler. Med-Orion, London, pp. 17–32
2. Belcaro GV, Hoffman U, Bollinger A, Nicolaides AN (eds) (1994) Laser Doppler. Med-Orion, London
3. Bonner RF, Nossal R (1981) Model for laser Doppler measurements of blood flow in tissue. Appl Opt 20:2097–2107
4. Bonner RF, Nossal R (1990) Principles of laser-Doppler flowmetry. In: Shepherd AP, Öberg PÅ (eds) Laser-Doppler blood flowmetry. Kluwer, Massachusetts, pp 17–45
5. Borgos J (1994) Principles of instrumentation: calibration and technical issues. In: Belcaro GV, Hoffman U, Bollinger A, Nicolaides AN (eds) Laser Doppler. Med-Orion, London, pp 3–16
6. Bracic Lotric M, Stefanovska A, Stajer D, Urbancic-Rovan V (2000) Spectral components of heart rate variability determined by wavelet analysis. Physiol Meas 21:441–457
7. Bracic M, Stefanovska A (1998) Wavelet-based analysis of human blood-flow dynamics. B Math Biol 60:919–935
8. Bracic M, Stefanovska A (1999) Wavelet analysis in studying the dynamics of blood circulation. Nonlinear Phenom Complex Syst 2:68–77
9. Briers JD, Richards G, He XW (1999) Capillary blood flow monitoring by laser speckle contrast analysis (Lasca). J Biomed Opt 4:164–175
10. Cummins HZ, Swinney HL (1970) Light beating spectroscopy. In: Wolf E (ed) Progress in optics. North-Holland, Amsterdam, pp 135–200
11. Duteil L, Bernengo J, Schalla W (1985) A double wavelength laser Doppler system to investigate skin microcirculation. IEEE Trans Biomed Eng BME 32:439–447
12. Essex TJ, Byrne PO (1991) A laser Doppler scanner for imaging blood flow in skin. J Biomed Eng 13:189–194
13. Forrester AT (1961) Photoelectric mixing as a spectroscopic tool. J Opt Soc Am 51:253–259
14. Forrester KR, Stewart C, Tulip J, Leonard C, Bray RC (2002) Comparison of laser speckle and laser Doppler perfusion imaging: measurement in human skin and rabbit articular tissue. Med Biol Eng Comput 40:687–697
15. Forrester KR, Tulip J, Leonard C, Stewart C, Bray RC (2004) A laser speckle imaging technique for measuring tissue perfusion. IEEE Trans Biomed Eng 51:2074–2084

16. Fredriksson I, Larsson M, Strömberg T (2006) Absolute flow velocity components in laser Doppler flowmetry. In: Proceedings of SPIE, San José, CA, vol 6094, 60940A, 12 p
17. Fromy B, Abraham P, Saumet JL (1998) Non-nociceptive capsaicin-sensitive nerve terminal stimulation allows for an original vasodilatory reflex in the human skin. Brain Res 811:166–168
18. Fromy B, Merzeau S, Abraham P, Saumet JL (2000) Mechanisms of the cutaneous vasodilator response to local external pressure application in rats: involvement of CGRP, neurokinins, prostaglandins and NO. Br J Pharmacol 131:1161–1171
19. Fromy B, Abraham P and Saumet JL (2000) Progressive calibrated pressure device to measure cutaneous blood flow changes to external pressure strain. Brain Res Protoc 5:198–203
20. Fromy B, Abraham P, Bouvet C, Bouhanick B, Fressinaud P, Saumet JL (2002) Early decrease of skin blood flow in response to locally applied pressure in diabetic subjects. Diabetes 51:1214–1217
21. Geyer MJ, Jan YK, Brienza DM, Boninger ML (2004) Using wavelet analysis to characterize the thermoregulatory mechanisms of sacral skin blood flow. J Rehabil Res Dev 41:797–806
22. Gush RJ, King TA, Jayson MI (1984) Aspects of laser light scattering from skin tissue with application to laser Doppler blood flow measurement. Phys Med Biol 29:1463–1476
23. Holloway GA, Watkins DW (1977) Laser Doppler measurement of cutaneous blood flow. J Invest Dermatol 69:306–309
24. Humeau A, Koitka A, Saumet J L and L'Huillier JP (2003) Dynamic characteristics of the cutaneous vasodilator response to a local external pressure application detected by the laser Doppler flowmetry technique on anaesthetised rats. In: Boas DA (ed) Photon migration and diffuse-light imaging. Proceedings of SPIE-OSA biomedical optics, SPIE 5138, pp 72–79
25. Humeau A, Koïtka A, Abraham P, Saumet JL, L'Huillier JP (2004) Time-frequency analysis of laser Doppler flowmetry signals recorded in response to a progressive pressure applied locally on anaesthetised healthy rats. Phys Med Biol 49:843–857
26. Humeau A, Koïtka A, Abraham P, Saumet JL, L'Huillier JP (2004) Spectral components of laser Doppler flowmetry signals recorded in healthy and type 1 diabetic subjects at rest and during a local and progressive cutaneous pressure application: scalogram analyses. Phys Med Biol 49:3957–3970
27. Humeau A, Koïtka A, Abraham P, Saumet JL, L'Huillier JP (2004) Dynamic characteristics of laser Doppler flowmetry signals obtained in response to a local and progressive pressure applied on diabetic and healthy subjects. In: Wyrowski F (ed) Photon management. Proceedings of SPIE, vol 5456, SPIE, Bellingham, WA, pp 307–314
28. Humeau A, Fizanne L, Garry A, Saumet JL, L'Huillier JP (2004) Signal processing methodology to study the cutaneous vasodilator response to a local external pressure application detected by laser Doppler flowmetry. IEEE Trans Biomed Eng 51:190–192
29. Johansson K, Jakobsson A, Lindahl K, Lindhagen J, Lundgren O, Nilsson GE (1991) Influence of fibre diameter and probe geometry on the measuring depth of laser Doppler flowmetry in the gastrointestinal application. Int J Microcirc Clin Exp 10:219–229
30. Kirsner RS, Haiken M, Garland LD (1993) Margin assessment of selected basal cell carcinomas utilizing laser Doppler velocimetry. Int J Dermatol 32:290–292
31. Koïtka A, Abraham P, Bouhanick B, Sigaudo-Roussel D, Demiot C, Saumet JL (2004) Impaired pressure-induced vasodilation at the foot in young adults with type 1 diabetes. Diabetes 53: 721–725
32. Kvandal P, Landsverk SA, Bernjak A, Stefanovska A, Kvernmo HD, Kirkeboen KA (2006) Low-frequency oscillations of the laser Doppler perfusion signal in human skin. Microvasc Res PMID: 16854436
33. Kvernmo HD, Stefanovska A, Bracic M, Kirkebøen KA, Kvernebo K (1998) Spectral analysis of the laser Doppler perfusion signal in human skin before and after exercise. Microvasc Res 56:173–182
34. Kvernmo HD, Stefanovska A, Bracic M, Kirkeboen KA, Kvernebo K (1998) Spectral analysis of the laser Doppler perfusion signal in human skin before and after exercise. Microvasc Res 56:173–182
35. Kvernmo HD, Stefanovska A, Kirkeboen KA, Kvernebo K (1999) Oscillations in the human cutaneous blood perfusion signal modified by endothelium-dependent and endothelium-independent vasodilators. Microvasc Res 57:298–309
36. Landsverk A, Kvandal P, Kjelstrup T, Benko U, Bernjak A, Stefanovska A, Kvernmo H, Kirkeboen KA (2006) Human skin microcirculation after brachial plexus block evaluated by wavelet transform of the laser Doppler flowmetry signal. Aesthesiology 105:478–484
37. Larsson M, Strömberg T (2006) Toward a velocity-resolved microvascular blood flow measure by decomposition of the laser Doppler spectrum. J Biomed Opt 11:14024–1-9
38. Larsson M, Steenbergen W, Strömberg T (2002) Influence of optical properties and fibre separation on laser Doppler flowmetry. J Biomed Opt 7:236–243
39. Meglinsky IV, Matcher SJ (2001) Modelling the sampling volume for skin blood oxygenation measurements. Med Biol Eng Comput 39:44–50
40. Moor Instruments Ltd (2001) Reference list, http://www.moor.co.uk Moor Instruments Ltd
41. de Mul FFM, van Spijker J, van der Plas D, Greve J, Aarnoudse JG, Smits TM (1984) Mini laser-Doppler (blood) flow monitor with diode laser source and detection integrated in the probe. Appl Opt 23:2970–2973
42. Nilsson GE (1984) Signal processor for Laser Doppler Tissue Flowmeters. Med Biol Eng Comput 22:343–348
43. Nilsson H (2002) Photon migration in tissue. Laser induced fluorescence for cancer diagnostics and influence of optical properties on microvascular Doppler spectroscopy. PhD Thesis, Faculty of health sciences, Linköpings Universitet
44. Nilsson GE, Tenland T, Öberg PÅ (1980) A new instrument for continuous measurement of tissue blood flow by light beating spectroscopy. IEEE Trans Biomed Eng BME 27:12–19
45. Nilsson GE, Tenland T, Öberg PÅ (1980) Evaluation of a laser Doppler flowmeter for measurement of tissue blood flow. IEEE Trans Biomed Eng BME 27:597–604
46. Nilsson GE, Jakobsson A, WÅrdell K (1989) Imaging of tissue blood flow by coherent light scattering, in IEEE 11th Ann EMBS Conf., Seattle, WA
47. Nilsson G, Jakobsson A, WÅrdell K (1991) Tissue perfusion monitoring and imaging by coherent light scattering. In: Soares ODD, Scheggi AM (eds) Bioptics: optics in biomedicine and environmental sciences, vol 1524, pp 90–109
48. Nilsson GE, Salerud EG, Strömberg T, WÅrdell K (2003) Laser Doppler perfusion monitoring and imaging. In: Vo-Dinh T (eds) Biomedical photonics handbook. CRC Press, Boca Raton
49. Öberg PÅ (1990) Laser-Doppler flowmetry. Crit Rev Biomed Eng 18:125–163
50. Perimed A (2001) Reference list, http://www.perimed.se Perimed AB
51. Rakotomamonjy A, Coast D, Marché P (1999) Wavelet-based enhancement of signal-averaged electrocardiograms for late potential detection. Med Biol Eng Comput 37:750–759
52. Riva C, Ross B, Benedek GB (1972) Laser Doppler measurements of blood flow in capillary tubes and retinal arteries. Invest Ophthalmol 11:936–944
53. Salerud EG, Nilsson GE (1986) Integrating probe for tissue laser Doppler flowmeters. Med Biol Eng Comput 24:415–419

54. Serov A, Steenbergen W, De Mul F (2001) Prediction of the photodetector signal generated by Doppler-induced speckle fluctuations: theory and some validations. J Opt Soc Am 18:622–630
55. Serov A, Steenbergen W, de Mul F (2002) Laser Doppler perfusion imaging with a complimentary metal oxide semiconductor image sensor. Opt Lett 27:300–302
56. Serov A, Steinacher B, Lasser T (2005) Full-field laser Doppler perfusion imaging and monitoring with an intelligent CMOS camera. Opt Express 13:3681–3689
57. Shepherd AP (1990) History of laser-Doppler blood flowmetry. In: Shepherd AP, Öberg PÅ (eds) Laser-Doppler blood flowmetry. Kluwer, Boston
58. Shepherd AP, Öberg PÅ (eds) (1990) Laser-Doppler blood flowmetry, Kluwer, Boston
59. Söderström T, Stefanovska A, Veber M, Svensson H (2003) Involvement of sympathetic nerve activity in skin blood flow oscillations in humans. Am J Physiol Heart Circ Physiol 284:H1638–1646
60. Stefanovska A, Bracic M and Kvernmo HD (1999) Wavelet analysis of oscillations in the peripheral blood circulation measured by laser Doppler technique. IEEE Trans Biomed Eng 46:1230–1239
61. Stern MD (1975) In vivo evaluation of microcirculation by coherent light scattering. Nature 254:56–58
62. Stern MD, Lappe DL, Bowen PD, Chimosky JE, Holloway GA, Keiser HR, Bowman RL (1977) Continuous measurement of tissue blood flow by laser-Doppler spectroscopy. Am J Physiol 232:H441–H448
63. Stücker M, Horstmann I, Nüchel C, Röchling A, Hoffmann K, Altmeyer P (1999) Blood flow compared in benign melanocytic naevi, malignant melanomas and basal cell carcinomas. Clin Exp Dermatol 24:107–111
64. Tur E, Brenner S (1992) Cutaneous blood flow measurements for the detection of malignancy in pigmented skin lesions. Dermatology 184:8–11
65. Urbancic-Rovan V, Bernjak A, Stefanovska A, Azman-Juvan K, Kocijancic A (2006) Macro- and microcirculation in the lower extrmities—possible relationship. Diabetes Res Clin Pract 73:166–173
66. Veber M, Bandrivskyy A, Clarkson PBM, McClintock PVE, Stefanovska A (2004) Wavelet analysis of blood flow dynamics: effect on the individual oscillatory components of iontophoresis wit pharmacologically neutral electrolytes. Phys Med Biol 49:N111-N117
67. WÅrdell K, Jakobsson A, Nilsson GE (1993) Laser Doppler perfusion imaging by dynamic light scattering. IEEE Trans Biomed Eng 40:309–316
68. Yuan S, Devor A, Boas DA, Dunn AK (2005) Determination of optimal exposure time for imaging of blood flow changes with laser speckle contrast imaging. Appl Opt 44:1823–1830